http://dx.doi.org/10.5012/bkcs.2014.35.8.2477

Simple Preparation of Anatase Titanium Dioxide Nanoparticles by Heating Titanium-Organic Frameworks

Ji Hyuk Im, Eunyoung Kang,† Seung Jae Yang, Hye Jeong Park,† Jaheon Kim,†,* and Chong Rae Park*

Carbon Nanomaterials Design Laboratory, Global Research Laboratory, Research Institute of Advanced Materials, and Department of Materials Science and Engineering, Seoul National University, Seoul 151-744, Korea
**E-mail: crpark@snu.ac.kr*
†Institute for Integrative Basic Sciences, Department of Chemistry, Soongsil University, Seoul 156-743, Korea
**E-mail: jaheon@ssu.ac.kr*
Received January 9, 2014, Accepted April 30, 2014

Thermal degradation of titanium–containing metal-organic frameworks (MOFs; MIL-125 and MIL-125-NH_2 at 350 °C for 6 h in air produced TiO_2 nanoparticles of *ca.* 10 nm in diameter. Scanning electron and transmission electron microscope analyses indicated that those nanoparticles were aggregated randomly within each crystalline particle of their MOF precursors. The TiO_2 nanoparticles prepared from MIL-125-NH_2 exhibited higher activity for the degradation of 4-chlorophenol under visible light.

Key Words : Metal-organic frameworks, Thermolysis, Titanium dioxide, Nanoparticles, MIL-125

Introduction

Metal–organic frameworks (MOFs) are extended structures with regular arrays of metal ions and organic linkers. Their pores are surrounded by framework metal ions and functional linkers, allowing MOFs to have specific functions for gas storage and separation, catalysis, sensing, or drug delivery.[1,2] MOFs are also used as host materials for various inorganic nanoparticles. Inclusion of molecular precursors in MOFs and their subsequent reduction provide metal nanoparticles embedded in MOF pores, as demonstrated in the production of Ag, Au, Pt, Pd, Cu, Ru, Ni, and PtRu nanoparticles.[2] In contrast to using the precursors, thermal decomposition of MOFs themselves under inert atmosphere results in porous carbon on which metal or metal oxide nanoparticles are supported.[3-8] Similar thermal treatments in air makes the organic units completely burn off, and provide metal oxide nanoparticles as residues. This simple and straightforward process has been successfully applied for making various binary and tertiary nanoparticles such as ZnO,[8-10] CuO,[9,11,13] Co_3O_4,[9,10,14,15] Mn_2O_3,[9,16] CdO,[9] MgO,[9] Mn_3O_4,[10] Al_2O_3,[17] In_2O_3,[18] and some spinel structures like $CoMn_2O_4$, $NiMn_2O_4$, and $ZnMn_2O_4$.[19] Thus, the regular and repetitive structures of various chemical compositions in MOFs enable them to act as versatile precursors for homogeneous and stoichiometric solid-state reactions.

Titanium dioxide can convert solar energy to generate electricity or can serve as a photocatalyst. Therefore, it has been extensively studied for dye-sensitized solar cells, water-splitting reactions, and removing organic pollutants.[20,21] However, due to large band gap only amenable to ultra violet illumination (for example, 3.2 eV for anatase at below 387 nm), extensive research efforts have been devoted to improve the photo-efficiency of TiO_2. Controlling both the size and shape of TiO_2 nanoparticles is one solution to reduce electron-hole recombination rates.[21] Extrinsic doping to modulate TiO_2 band gaps has been also explored by various chemical methods. This approach is effective in enhancing the visible light activity of TiO_2 by doping extrinsic metal atoms such as Cr, V, Fe, Co, and Mo or non-metals (B, C, N, F, P, S).[21-23] Among them, N has a same atomic size as that of O, which facilitates its doping in TiO_2 under mild sol-gel reaction conditions. A variety of nitrogen sources are available as dopant precursors such as nitrate, aliphatic amines,

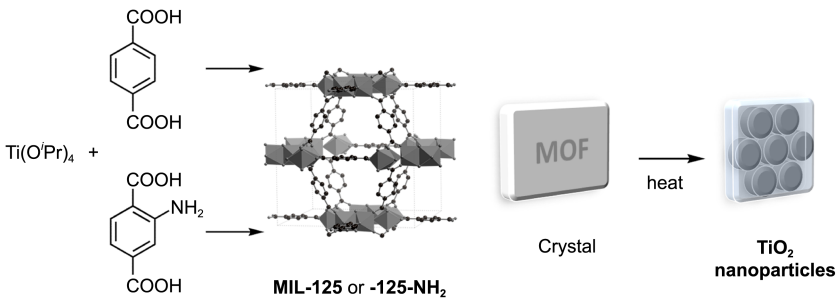

Scheme 1. Steps for the production of the aggregated TiO_2 nanoparticles by the thermal decomposition of MIL-125 or MIL-125-NH_2 crystals.

ammonia, ammonium salts, or urea.[24-27] In spite of the current debate on the origin or mechanism,[23] N-doped TiO_2 materials are known to show significant visible light activity compared to unmodified TiO_2.[24-29]

Here, we report the simple preparation of TiO_2 nanoparticles under an air atmosphere using thermal decomposition of two MOFs, MIL-125 and MIL-125-NH_2 (Scheme 1). MIL-125 is the first porous MOF synthesized by Ti ions as metal ions, and formulated as $Ti_8O_8(OH)_4(BDC)_6$ (BDC = benzene-1,4-dicarboxylate).[30]

This MOF has fused eight TiO_6 octahedron units connected by BDC linkers to form a three-dimensional microporous framework. MIL-125-NH_2 has the same structure as MIL-125 as the BDC-NH_2 linkers play the same structural role as the BDCs in MIL-125.[31] It was anticipated that the thermal decomposition of the MOF crystals would give TiO_2 nanoparticles, and in particular, MIL-125-NH_2 would act as a precursor for N-doped TiO_2 nanoparticles. For simplicity in this work, MIL-125 and MIL-125-NH_2 are termed 1 and 2, respectively.

Experimental

Synthesis. MIL-125 (**1**) was prepared by following the literature method,[30] Titanium(IV) isopropoxide ($Ti(O^iPr)_4$, 0.60 mL, 2.0 mmol) and H_2BDC (0.50 g, 3.0 mmol) were put into a mixed solvent system of *N*,*N*-dimethylformamide (DMF, 9.0 mL) and methanol (1.0 mL). The reaction mixture was then stirred at ambient temperature for 30 min to make a homogeneous solution. The clear solution was transferred to a 23-mL Teflon vessel in a digestion bomb. The reactor was tightly capped and heated at 150 °C for 18 h yielding a white crystalline powder. The solid was filtered and washed with neat DMF (5 × 10 mL) and methanol (3 × 10 mL) before drying under reduced pressure. MIL-125-NH_2 (**2**) was synthesized according to the published procedure.[31] $Ti(O^iPr)_4$ (2.0 mL, 6.7 mmol) and H_2BDC-NH_2 (2.0 g, 11 mmol) were put in a mixed solvent system of DMF (50 mL) and methanol (50 mL). Unlike the case of MIL-125, the reaction mixture did not turn into a homogeneous solution. The reaction mixture was then transferred to a 300-mL Teflon vessel in a digestion bomb. The reactor was tightly capped and heated at 150 °C for 24 h yielding a dark-yellow crystalline powder. The solid was filtered and washed with neat DMF (5 × 10 mL) and methanol (3 × 10 mL) before drying under reduced pressure. TiO_2 nanoparticles were prepared by heating **1** or **2** at constant temperature. **1** or **2** was put into a zirconia crucible and heated in a furnace at 350 °C in air for 6 h to prepare TiO_2 nanoparticles, TiO_2(**1**) or TiO_2(**2**), respectively.

Characterization. Powder X-ray diffraction (PXRD) patterns were measured on a Rigaku Miniflex diffractometer with CuKα (λ = 1.5418 Å) radiation. Thermogravimetric analyses (TGA) were performed on a TA SDT Q600 with a temperature change of 10 ºC/min. Nitrogen adsorption isotherms were measured on an ASAP 2020 (Micrometrics, USA) at 77 K. Before measurements, the samples were activated at 180 ºC for 12 h. Specific surface areas were calculated according to the Brunauer–Emmett–Teller (BET) equation with isotherm points under $P/P_0 < ca.$ 0.1. Scanning electron microscopy (SEM) images were obtained on a JSM-6330F (JEOL, Japan) with accelerating voltage of 10 kV. Transmission electron microscopy (TEM) measurements were carried out on a FEI Tecnai F20 microscope (JEOL, Japan) with accelerating voltage of 200 kV. X-ray photoelectron spectroscopy (XPS) spectra were collected on an AXIS-Hsi (Kratos, UK) (delay line detector) spectrometer equipped with a monochromatic Al K? X-ray source (1486.6 eV).

Photocatalytic Activity Measurement. The general procedure is the same as that in the previous article on the photocatalytic activity of ZnO nanoparticles obtained by thermolysis of MOF-5.[8] The photocatalytic properties of TiO_2 nanoparticles in this work were evaluated by conducting photodegradation of 4-chlorophenol. Each TiO_2 sample (25 mg) was added to a 20 mL 4-chlorophenol aqueous solution with an initial concentration of 2.5×10^{-4} M. With a time interval of 2 h for UV (20 W, Shimadzu) or 20 min for visible light (100 W, Philips, UV-cut filter) experiments, the sample solution was taken after filtering through a 0.2 μm hydrophilic PTFE syringe filter. The concentration of 4-chlorophenol was calculated as a function of time based on the absorbance changes at λ = 250 nm measured on a UV-Vis spectrophotometer (Cary 5000, Varian). The commercial TiO_2 P-25 (Evonik) and ST-01 (Ishihara) were used as reference materials.

Results and Discussion

Two Ti-MOFs, **1** and **2**, were synthesized as rectangular microcrystals with average sizes of *ca.* 500 nm and 1 μm, respectively, as seen in their SEM images (Figure S1). The plate-like crystals of **1** and **2** are distinguishable from each other because the former has round surfaces and the latter has sharp edges. As expected the PXRD patterns of both **1** and **2** matched each other, and also were well-matched to the reported patterns of MIL-125 (Figure S2). The nitrogen adsorption isotherms of **1** and **2** showed type I isotherms (Figure S3). The BET surface areas for **1** and **2** are estimated to be 1550 and 1450 m^2/g, respectively, which are nearly the same as the reported values.[30,31] TGA analyses showed that both MOFs started to lose weight at around 300 °C in air due to the thermal degradation of their organic linkers. However, **1** showed a large weight loss at 400 °C whereas **2** did at a much lower temperature, about 330 °C (Figure S4).

When **1** and **2** were respectively heated at 350 ºC for 6 h *in air*, PXRD patterns indicated the production of anatase TiO_2 particles (termed TiO_2(**1**) and TiO_2(**2**)) (Figure 1(a)). Both the TiO_2(**1**) and TiO_2(**2**) particles gave the same PXRD intensity distributions, implying that their particle sizes and shapes are almost similar to each other. Although **1** and **2** were heated at temperatures much higher than those in common sol-gel preparations (< 200 ºC) of TiO_2,[21,26] the TGA traces in Figure S4 indicate that two MOFs are not

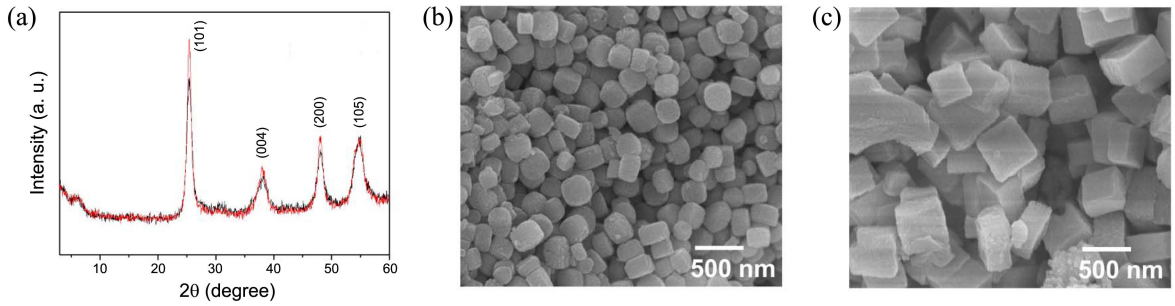

Figure 1. (a) Overlapped PXRD patterns of TiO_2(**1**) and (c) TiO_2(**2**), and SEM images of (b) TiO_2(1) and (c) TiO_2(**2**).

completely decomposed at that temperature, indicating that the TiO_2 particles might be blended with the unidentified amorphous residues of their MOF precursors. It was interesting that further heating at 400 ºC a rutile phase for TiO_2(**1**) was observed, but not for TiO_2(**2**) (not shown). The SEM images showed that TiO_2(**1**) formed as thick rectangular plates with *ca.* 200 nm in their sizes (Figure 1(b)). In contrast, TiO_2(**2**) particles are sharp rectangles with a larger size, *ca.* 500 nm (Figure 1(c)). However, these sizes are larger than the values calculated from their PXRD patterns. Based on the Sherrer equation using (101) reflections in the PXRD patterns in Figure 2(a), the particle sizes were calculated to be *ca.* 10 nm for both TiO_2(**1**) and TiO_2(**2**) particles. Considering that the TiO_2 nanoparticles in TiO_2(**1**) and TiO_2(**2**) show similar sizes and a same anatase phase, the aggregate sizes seem to be related to the crystal sizes of their MOF precursors.

In order to understand the size discrepancy between PXRD patterns and SEM image analyses, the TEM images for the TiO_2 particles were obtained (Figure 2). The TEM images of the TiO_2(**1**) and TiO_2(**2**) clearly showed that each

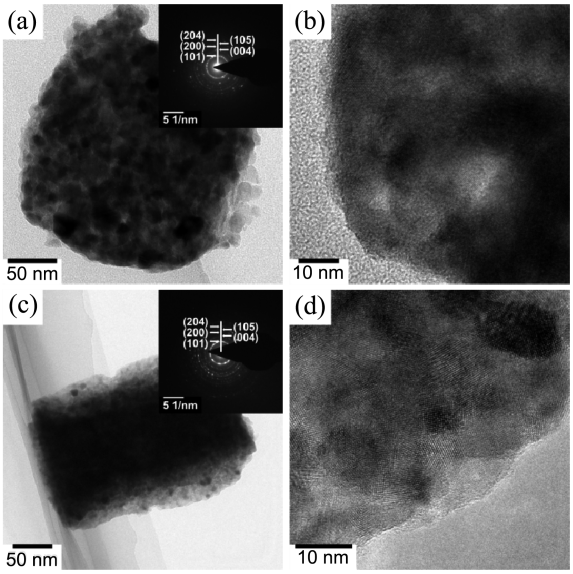

Figure 2. (a and b) TEM images of TiO_2(1) (inset : SAED pattern); (c and d) TEM images of TiO_2(2) (inset : SAED pattern). The images (b) and (d) show random aggregation of small nanoparticles with about 10 nm domains.

TiO_2 particle is not a single crystal but an aggregate composed of randomly oriented ~10 nm TiO_2 particles (Figure 2(b), 2(d)). High resolution images also showed the lattice fringes of each nanoparticle corresponding to the d-spacing of a (110) crystallographic plane (0.36 nm), which is also supported by the electron diffraction pattern (SAED, the insets in Figure 2). It is interesting that those ~10 nm particles are aggregated to form bigger particles exhibiting well-developed surfaces, which is similar to their MOF precursor crystals. This implies that the formation of TiO_2 nanoparticles happened inside each particle rather than involving inter-particle reactions.[10,11] This observation is in line with the previous reports that the shape of carbonized products tends to follow the original morphology of their MOF precursors.[8] That is, the 10 nm TiO_2 nanoparticles form within each MOF crystal during the thermal decomposition, and become aggregated and stabilized with maintaining the original morphology of the MOF crystal.

The photocatalytic activities of the TiO_2 particles were tested by conducting the decomposition reactions of 4-chlorophenol in water under UV and visible light and compared with those of commercial nanoparticles, P-25 and ST-01. Under UV, the TiO_2 particles in this work showed moderate activity compared with the commercial nanoparticles; P-25 and ST-01 made 4-chlorophenol degrade by 80% and 40%, respectively while TiO_2(**1**) and TiO_2(**2**) caused 60%

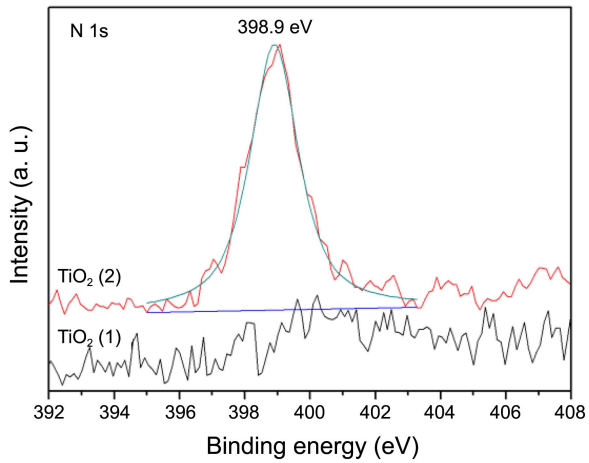

Figure 3. High-resolution N 1s XPS spectra of TiO_2(**1**) and TiO_2(**2**).

and 15% degradation of the 4-chlorophenol molecule, respectively (Figure S5a, S5b). However, under visible light (> 400 nm), the TiO_2(**2**) showed significantly enhanced photocatalytic activity for the decomposition of 4-chlorophenol among the used TiO_2 samples (Figure S5c, S5d). Considering that the aggregation of the TiO_2(**2**) nanoparticles limited their exposure to aqueous solutions, the enhanced photocatalytic efficiency under visible light is noticeable.

The enhancement of the visible light activity of TiO_2(**2**) might be related to the decrease in the band gap energy, which is shown for the N-doped TiO_2 particles prepared by employing organic amine molecules as nitrogen sources.[25-29] While the XPS spectrum of TiO_2(**1**) did not show any peaks corresponding to N 1s, the TiO_2(**2**) resulted in a signal at 398.9 eV indicating the presence of doped N atoms in TiO_2(**2**) (Figure 3). However, the ICP-AES analyses did not show any quantitative evidence on the N atoms in the acid-digested sample for TiO_2(**2**). This inconsistent observation suggests a possibility that during the thermal treatment of **2**, the framework was not completely decomposed and N atoms might have been present in the form of $-NH_2$ or the N-dopants in the carbonaceous solid, along with TiO(**2**). Thus, the acid-digestion might not able to dissolve out the N-containing species. Or, at current, we also rule out the possibility of the production of N-doped TiO(**2**) even if we could not get a quantitative analysis result. We will continue further investigation to verify the origin of the enhanced visible light activity of TiO(**2**).

Conclusion

Anatase TiO_2 nanostructures were simply prepared by heating **1** (or MIL-125) and **2** (or MIL-125-NH_2) at 350 ºC for 6 h under air. The TiO_2(**1**) and TiO_2(**2**) with an average size of ~200 or 500 nm, respectively, are composed of randomly oriented ~10 nm TiO_2 particles. TiO_2(**2**) showed an enhanced visible light activity in the photocatalytic degradation of 4-chlorophenol.

Acknowledgments. This research was supported by a grant from the Fundamental R&D Program for Core Technology of Materials funded by the Ministry of Knowledge Economy, Republic of Korea (C.R.P.), and by the Korea CCS R&D Center (KCRC) grant funded by the Korea government (NRF-2012-0008900) (J.K.).

Supporting Information. SEM images, PXRD patterns, N_2 sorption isotherms, and TGA traces of **1** and **2**, and the results for the phtocatalytic degradation reactions of 4-chloro phenol are provided. This material is available free of charge *via* the Internet at http://kcsnet.or.kr.

References

1. Kuppler, R. J.; Timmons, D. J.; Fang, Q.-R.; Li, J.-R.; Makal, T. A.; Young, M. D.; Yuana, D.; Zhao, D.; Zhuang, W.; Zhou, H.-C. *Coord. Chem. Rev.* **2009**, *253*, 3042.
2. Jiang, H.-L.; Xu, Q. *Chem. Commun.* **2011**, *47*, 3351 and references therein.
3. Jiang, H.-L.; Liu, B.; Lan, Y.-Q.; Kuratani, K.; Akita, T.; Shioyama, H.; Zong, F.; Xu, Q. *J. Am. Chem. Soc.* **2011**, *133*, 11854.
4. Liu, B.; Shioyama, H.; Jiang, H.; Zhang, X.; Xu, Q. *Carbon* **2012**, *48*, 456.
5. Hu, J.; Wang, H.; Gao, Q.; Guo, H. *Carbon* **2010**, *48*, 599.
6. Yuan, D.; Chen, J.; Tan, S.; Xia, N.; Liu, Y. *Electrochem. Commun.* **2009**, *11*, 1191.
7. Liu, B.; Shioyama, H.; Akita, T.; Xu, Q. *J. Am. Chem. Soc.* **2008**, *130*, 5390.
8. Yang, S. J.; Im, J. H.; Kim, T.; Lee, K.; Park, C. R. *J. Hazard. Mater.* **2011**, *186*, 376.
9. Das, R.; Pachfule, P.; Banerjee, R.; Poddar, P. *Nanoscale* **2012**, *4*, 591.
10. Zhao, J.; Li, M.; Sun, J.; Liu, L.; Su, P.; Yang, Q.; Li, C. *Chem. Eur. J.* **2012**, *18*, 3163.
11. Fan, Y.; Liu, R.; Du, W.; Lu, Q.; Pang, H.; Gao, F. *J. Mater. Chem.* **2012**, *22*, 12609.
12. Zamaro, J. M.; Perez, N. C.; Miro, E. E.; Casado, C.; Seoane, B.; Tellez, C.; Coronas, J. *Chem. Eng. J.* **2012**, *195-196*, 180.
13. Chen, L.; Zhao, C.; Wei, Z.; Wang, S.; Gu, Y. *Mater. Lett.* **2011**, *65*, 446.
14. Wang, W.; Li, Y.; Zhang, R.; He, D.; Liu, H.; Liao, S. *Catal. Commun.* **2011**, *12*, 875.
15. Liu, B.; Zhang, X.; Shioyama, H.; Mukai, T.; Sakai, T.; Xu, Q. *J. Power Sources* **2010**, *195*, 857.
16. Li, C. C.; Mei, L.; Chen, L. B.; Li, Q. H.; Wang, T. H. *J. Mater. Chem.* **2012**, *22*, 4982.
17. Parast, M. S. Y.; Morsali, A. *Inorg. Chem. Commun.* **2011**, *14*, 645.
18. Parast, M. S. Y.; Morsali, A. *Inorg. Chem. Commun.* **2011**, *14*, 450.
19. Zhao, J.; Wang, F.; Su, P.; Li, M.; Chen, J.; Yang, Q.; Li, C. *J. Mater. Chem.* **2012**, *22*, 13328.
20. Fujishima, A.; Rao, T. N.; Tryk, D. A. *J. Photochem. Photobio. C: Photochem. Rev.* **2000**, *1*, 1.
21. Chen, X.; Mao, S. S. *Chem. Rev.* **2007**, *107*, 2891.
22. Pelaez, M.; Nolan, N. T.; Pillai, S. C.; Seery, M. K.; Falaras, P.; Kontos, A. G.; Dunlop, P. S. M.; Hamilton, J. W. J.; Byrne, J. A.; O'Shea, K.; Entezari, M. H.; Dionysiou, D. D. *Appl. Catal. B: Environ.* **2012**, *125*, 331.
23. Emeline, A. V.; Kuznetsov, V. N.; Rybchuk, V. K.; Serpone, N. *Int. J. Photoenergy* **2008**, *2008*, 258394.
24. Mitoraj, D.; Kisch, H. *Chem. Eur. J.* **2012**, *16*, 261.
25. Jagadale, T. C.; Takale, S. P.; Sonawane, R. S.; Joshi, H. M.; Patil, S. I.; Kale, B.; Ogale, S.B. *J. Phys. Chem. C* **2008**, *112*, 14595.
26. Cong, Y.; Zhang, J.; Chen, F.; Anpo, M. *J. Phys. Chem. C* **2007**, *111*, 6976.
27. Qiu, X.; Zhao, Y.; Burda, C. *Adv. Mater.* **2007**, *19*, 3995.
28. Zhang, J.; Wu, Y.; Xing, M.; Leghari, S. A. K.; Sajjad, S. *Energy Environ. Sci.* **2010**, *3*, 715.
29. Izumi, Y.; Itoi, T.; Peng, S.; Oka, K.; Shibata, Y. *J. Phys. Chem. C* **2009**, *113*, 6706.
30. Dan-Hardi, M.; Serre, C.; Frot, T.; Rozes, L.; Maurin, G.; Sanchez, C.; Férey, G. *J. Am. Chem. Soc.* **2009**, *131*, 10857.
31. Zlotea, C.; Phanon, D.; Mazaj, M.; Heurtaux, D.; Guillerm, V.; Serre, C.; Horcajada, P.; Devic, T.; Magnier, E.; Cuevas, F.; Férey, G.; Llewellyn, P. L.; Latroche, M. *Dalton Trans.* **2011**, *40*, 4879.